THE ASTRONOMICAL JOURNAL, 122:1238–1250, 2001 September

STATISTICAL PROPERTIES OF BRIGHT GALAXIES IN THE SLOAN DIGITAL SKY SURVEY PHOTOMETRIC SYSTEM[1]

KAZUHIRO SHIMASAKU,[2] MASATAKA FUKUGITA,[3,4] MAMORU DOI,[5] MASARU HAMABE,[5] TAKASHI ICHIKAWA,[6] SADANORI OKAMURA,[2] MAKI SEKIGUCHI,[3] NAOKI YASUDA,[7] JON BRINKMANN,[8] ISTVÁN CSABAI,[9,10] SHIN-ICHI ICHIKAWA,[7] ZELJKO IVEZIĆ,[11] PETER Z. KUNSZT,[9] DONALD P. SCHNEIDER,[12] GYULA P. SZOKOLY,[13] MASARU WATANABE,[14] AND DONALD G. YORK[15]

Received 2001 January 22; accepted 2001 May 14

ABSTRACT

We investigate the photometric properties of 456 bright galaxies using imaging data recorded during the commissioning phase of the Sloan Digital Sky Survey (SDSS). Morphological classification is carried out by correlating results of several human classifiers. Our purpose is to examine the statistical properties of color indices, scale lengths, and concentration indices as functions of morphology for the SDSS photometric system. We find that $u'-g'$, $g'-r'$, and $r'-i'$ colors of SDSS galaxies match well with those expected from the synthetic calculation of spectroscopic energy distribution of template galaxies and with those transformed from $UBVR_CI_C$ color data of nearby galaxies. The agreement is somewhat poor, however, for the $i'-z'$ color band, with a discrepancy of 0.1–0.2 mag. With the aid of the relation between surface brightness and radius obtained by Kent in 1985, we estimate the averages of the effective radius of early-type galaxies and the scale length of exponential disks both to be 2.6 kpc for L^* galaxies. We find that the half-light radius of galaxies depends slightly on the color bands, consistent with the expected distribution of star-forming regions for late-type galaxies and with the known color gradient for early-type galaxies. We also show that the (inverse) concentration index, defined by the ratio of the half-light Petrosian radius to the 90% light Petrosian radius, correlates tightly with the morphological type; this index allows us to classify galaxies into early (E/S0) and late (spiral and irregular) types, allowing for a 15%–20% contamination from the opposite class compared with eye-classified morphology.

Key words: galaxies: fundamental parameters — galaxies: photometry

1. INTRODUCTION

The Sloan Digital Sky Survey (SDSS; York et al. 2000) has started producing both photometric and spectroscopic data. It is expected that the SDSS will produce a very large and homogeneous database for research on the nature of galaxies. Photometric observations are made with the new five color bands (u', g', r', i', and z') that divide the entire range from the atmospheric ultraviolet cutoff to the sensitivity limit of silicon CCD into five essentially nonoverlapping passbands (Fukugita et al. 1996). These passbands are chosen on the basis of their astrophysical merits, but this specific choice makes it difficult to compare or combine the SDSS data with those obtained with more conventional photometric systems.

In this paper, we present results from a brief analysis for properties of galaxies using a small set of data for bright galaxies in the new photometric system. The present results have already been used to construct empirical galaxy models for simulations that have been used extensively to tune the SDSS project software (Lupton et al. 2001) and to aid galaxy science (Yasuda et al. 2000).

To study properties of galaxies, it is essential to classify the galaxies into morphological types, since different morphological types exhibit distinctly different astrophysical properties, reflecting the different histories of the formation and evolution of galaxies. A number of attempts have been proposed for automated classification of morphologies (e.g., Doi, Fukugita, & Okamura 1993; Lahav et al. 1996; Abraham et al. 1994, 1996), but visual classification still serves as the most reliable method when we adopt the Hubble classification (Sandage 1961) for galaxies with large apparent sizes. This visual inspection procedure, which is, of course, very labor intensive, limits the size of our sample. While we are conducting an attempt to produce a large-scale eye-classified sample, we present here an analysis we have carried out as our initial study.

[1] Based on observations obtained from the Sloan Digital Sky Survey. Information available at http://www.sdss.org. Funding for the creation and distribution of the SDSS Archive has been provided by the Alfred P. Sloan Foundation, the Participating Institutions, the National Aeronautics and Space Administration, the National Science Foundation, the US Department of Energy, the Japanese Monbukagakusho, and the Max Planck Society.

[2] Department of Astronomy and Research Center for the Early Universe, School of Science, University of Tokyo, Tokyo, 113-0033 Japan.
[3] Institute for Cosmic-Ray Research, University of Tokyo, Kashiwa 277-8582, Japan.
[4] Institute for Advanced Study, Olden Lane, Princeton, NJ 08540.
[5] Institute of Astronomy, School of Science, University of Tokyo, Mitaka, Tokyo 181-0015, Japan.
[6] Astronomical Institute, Tohoku University, Sendai 980-8578, Japan.
[7] National Astronomical Observatory, 2-21-1, Mitaka, Tokyo 181-8588, Japan.
[8] Apache Point Observatory, P.O. Box 59, Sunspot, NM 88349-0059.
[9] Department of Physics and Astronomy, Johns Hopkins University, 3701 San Martin Drive, Baltimore, MD 21218.
[10] Department of Physics of Complex Systems, Eötvös University, Pázmány Péter sétány 1/A, Budapest, H-1117, Hungary.
[11] Princeton University Observatory, Princeton, NJ 08544.
[12] Department of Astronomy and Astrophysics, Pennsylvania State University, University Park, PA 16802.
[13] Astrophysikalisches Institut Potsdam, An der Sternwarte 16, 14482 Potsdam, Germany.
[14] The Institute of Space and Astronautical Science, Sagamihara, Kanagawa 229-8510, Japan.
[15] Astronomy and Astrophysics Center, University of Chicago, 5640 South Ellis Avenue, Chicago, IL 60637.

In this paper, we focus our considerations on three statistical quantities: color, effective size, and concentration parameter. Galaxy colors are an important quantity that characterizes stellar contents of galaxies. The colors at zero redshift are also used as a fiducial zero point to study statistical properties of faint galaxies and their evolution. An important test is to confirm whether the colors obtained with SDSS photometry are consistent with those expected from broadband photometry using the conventional passbands, B, V, R, and I and with those calculated from template spectroscopic energy distributions of galaxies. This is an initial step in establishing a photometric system where the spectrophotometrically synthesized flux matches closely with the broadband flux, which is one of the goals of SDSS photometry.

The second statistical quantity is the distribution of effective sizes of galaxies. The de Vaucouleurs profile (de Vaucouleurs 1948) is usually characterized by the half-light radius r_e and the exponential disk by the scale length h. These parameters set the fundamental length scales of galaxies. How these quantities scale with magnitude is indispensable information for construction of simulations of galaxies, in particular the study of the detectability of galaxies at faint magnitudes and the performance of star galaxy classification algorithms, both of which depend on the apparent sizes of galaxies. It is also interesting to ask whether the effective size varies across the different color bands, which provides information needed to understand the statistical distribution of stellar populations in galaxies for a global sample.

The third quantity we study is the concentration index of the light distribution of each galaxy. This parameter is known to correlate with the morphological type (Morgan 1958); earlier type galaxies have light profiles more concentrated toward the center. There is some evidence that this parameter can be used for automated morphological classification (Doi et al. 1993; Abraham et al. 1994). Specifically, we study the performance of automated classification schemes when the concentration parameter is used to classify galaxies into early and late types.

We describe briefly the data and the photometric catalog in § 2. In § 3, our morphological classification and the resulting catalog are described. Color indices are studied in § 4. In § 5, the distribution of the scale lengths of galaxies is discussed; and in § 6, the concentration index is studied. Conclusions are given in § 7.

2. OBSERVATION AND PHOTOMETRIC CATALOG

The SDSS (York et al. 2000) is carried out using a wide-field 2.5 m telescope, a large-format imaging camera (Gunn et al. 1998), two fiber-fed double spectrographs, and an auxiliary 0.5 m telescope for photometric calibration. The sky is imaged with 30 photometric CCDs arranged in six columns of five rows, each row corresponding to a different passband. The data are taken in time-delay-and-integrate mode at the sidereal rate along great circles on the sky, yielding a *strip* consisting of six very long and narrow *scan lines*, each 13.5 wide. The effective exposure time is 54.1 s. The scan lines of a given strip do not overlap, but observing a second strip offset from the first strip by about 12.8 gives a filled *stripe* 2.5 wide. The pixels are 0.396 square on a side. The 0.5 m Photometric Telescope observes standard stars to determine the atmospheric extinction on each night and ties the standard stars to objects observed with the 2.5 m survey telescope. SDSS imaging data taken in five passbands, u', g', r', i' and z' (Fukugita et al. 1996) are processed with the photometric pipeline (hereafter PHOTO; Lupton et al. 2001) specifically written for SDSS imaging data processing.

The galaxies used in this paper are taken from observations of the northern equatorial stripe on 1999 March 19 (SDSS run 745), supplemented with observations on 1999 March 20 (run 752) and 1999 March 21 (run 756). These imaging data were taken before the commissioning of the current Photometric Telescope. We calibrated the data by observing secondary patches in the survey area, using a (now decommissioned) 61 cm telescope at the observatory site, and by observing primary standard stars using US Naval Observatory's 40 inch (1 m) telescope, with filter and CCD characteristics nominally identical to those at the SDSS Photometric Telescope. Since the transformation from the primary standard stars to the objects observed with the SDSS 2.5 m telescope has not yet been fully defined, we expect photometric errors of $\approx \pm 0.05$ mag in each band with respect to the proper SDSS photometric system. Thus, in this paper, we will denote our magnitudes as u^*, g^*, r^*, i^*, and z^* to emphasize the preliminary nature of our photometric calibration, rather than the notation u', g', r', i', and z' that will be used for the final SDSS photometric system. However, we will use the latter notation to refer to the SDSS photometric passbands themselves. The magnitudes we use are based on the AB_{95} system (Fukugita et al. 1996).

The galaxies we study in this paper are taken from run 745, which ranges from R.A. $= 10^h41^m$ to 16^h41^m, covering effectively 127 deg^2 in total. We take all 217 galaxies brighter than $m_P(g^*) = 16$ mag contained in run 745 for morphological classification by eye [here $m_P(g^*)$ stands for the Petrosian magnitude in the g' band as defined below]. Additionally, we take all 160 galaxies with $16 \leq m_p(g^*) < 17$ in the R.A. range 10^h41^m to 11^h41^m and 107 galaxies with $17 \leq m_p(g^*) < 18$ in the R.A. range 10^h41^m to $10^h44^m.5$. This makes the size of our morphologically classified sample to be 484 galaxies in total. Our sample is not homogeneous with respect to brightness, but otherwise we do not expect any other selection biases. Those galaxies which fall on the edge of the fields are not taken in our sample. The g' band is used in order to facilitate comparison of our morphological classification with the work done in the past, which has been almost exclusively performed using the blue-band image.

After we carried out morphological classification using run 745, an improved photometric data processing was done for runs 752 and 756, the regions of which overlap with that of run 745. Therefore, we identified galaxies in our sample with those imaged by runs 752 and 756 and developed a photometric catalog from these two runs.[16] Unfortunately, the entire region of run 745 is not covered with runs 752 and 756, and this leads us to drop 28 galaxies. Hence, we work with 456 galaxies in the analysis given in this paper. Details of photometry of galaxies in runs 752 and 756 are discussed in Yasuda et al. (2000).

While many photometric parameters are measured in PHOTO, we are concerned in this paper only with three classes of parameters:

[16] We used PHOTO version 5.0.3 of late 1999. The most important improvement that concerns us here is in the accuracy of fluxes of deblended objects.

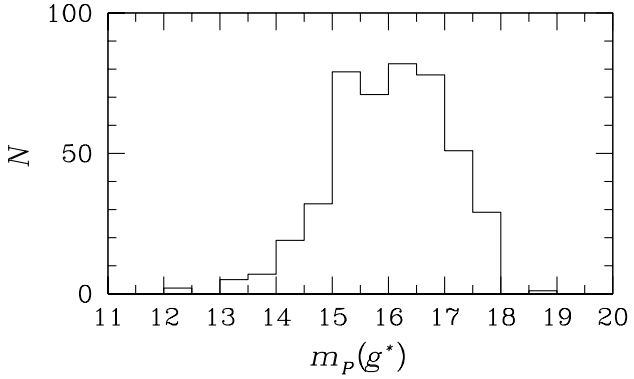

FIG. 1.—Distribution of Petrosian magnitudes in the g' band for the 456 galaxies analyzed in this paper. Magnitudes are corrected for Galactic extinction.

1. *Petrosian radius in the five bands*: $r_P(u')$, $r_P(g')$, $r_P(r')$, $r_P(i')$, $r_P(z')$. The Petrosian radius r_P is defined as the parameter that satisfies

$$\eta = \frac{I(r_P)}{2\pi \int_0^{r_P} I(r)rdr/(\pi r_P^2)} . \quad (1)$$

In practice, this implicit equation for r_P is replaced with

$$\eta = \frac{2\pi \int_{0.8r_P}^{1.25r_P} I(r)rdr/\{\pi[(1.25r_P)^2 - (0.8r_P)^2]\}}{2\pi \int I(r)rdr/(\pi r_P^2)} , \quad (2)$$

where $I(r)$ is the surface-brightness profile of the object. We adopt $\eta = 0.2$. We measure the Petrosian radius in each band, but we use only the radius measured in the r' band to calculate the Petrosian flux (or Petrosian magnitude) for all color bands, so that the aperture for the Petrosian flux is common to the five passbands.

2. *Petrosian magnitude in the five passbands*: $m_P(u')$, $m_P(g')$, $m_P(r')$, $m_P(i')$, $m_P(z')$. The Petrosian flux is defined as

$$F_P = 2\pi \int_0^{kr_P} I(r)rdr , \quad (3)$$

where k is set equal to 2 and r_P is the r' Petrosian radius. For further detailed discussion of the Petrosian flux, see Yasuda et al. (2000).

3. *Petrosian half-light radius and Petrosian 90% light radius*: $r_{50}(\lambda_i)$, $r_{90}(\lambda_i)$. The definitions of r_{50} and r_{90}, respectively, are such that the fluxes over the aperture with these radii are 50% and 90% of the Petrosian flux in the passband $\lambda_i = u', g', r', i'$, and z'.

To give an idea about the basic properties of our sample, we show the distribution of g'-band Petrosian magnitudes in Figure 1 and those of $r_P(r')$, $r_{50}(r')$, and $r_{90}(r')$ in Figure 2. Magnitudes are corrected for Galactic extinction using the dust distribution estimated by Schlegel, Finkbeiner, & Davis (1998) with the ratio of total to selective extinction $R_{g'} = 3.79$ and $R_{r'} = 2.75$. When necessary we use $R_{u'} = 5.2$, $R_{i'} = 2.09$, and $R_{z'} = 1.48$ for the other color bands.

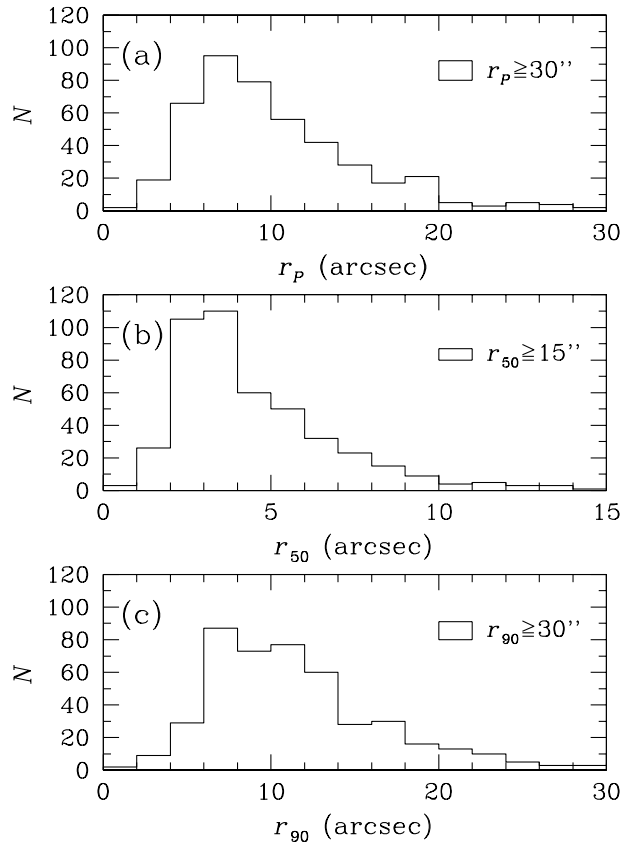

FIG. 2.—Distributions of Petrosian radii, Petrosian half-light radii, and Petrosian 90% light radii of the 456 galaxies measured for r'-band images.

3. MORPHOLOGICAL CLASSIFICATION

The galaxies in our sample are classified into seven morphological classes, $T = 0$ (corresponding to E in the Hubble type, or -5 in RC3 type), 1 (S0, $T_{RC3} = -3$ to -1), 2 (Sa, $T_{RC3} = 1$), 3 (Sb, $T_{RC3} = 3$), 4 (Sc, $T_{RC3} = 5$), 5 (Sdm, $T_{RC3} = 8$), and 6 (Im, $T_{RC3} = 10$), where T_{RC3} refers to the type index defined in the Third Reference Catalogue of Bright Galaxies (de Vaucouleurs et al. 1991, hereafter RC3). This classification is coarser than the standard RC3 types, but we consider that our classification is sufficient for most purposes for galaxy science. Four of the present authors (M. H., T. I., S. O., and M. S.) independently classified all galaxies by eye, by comparing the image of each galaxy displayed on the SAO image viewer with template galaxies of Frei & Gunn (1994) which are given morphological types by RC3. The templates of Frei & Gunn cover from E to Im. When one cannot assign a morphology to a galaxy, an index of -1 is given. For each galaxy, we adopt a median of four classifiers as the final value of T (a half integer means that the median falls in the middle). In finding a median, we ignore $T = -1$ when one or two classifiers give this index (no galaxy was given -1 by more than two classifiers). In this way some galaxies are given half-integer values of T. The catalog will be published elsewhere (Fukugita et al. 2001).

We have identified the 54 galaxies listed in RC3 and in run 745. Figure 3 compares our morphology T(ours) with that given in RC3, T_{RC3}, for the 54 galaxies. The size of the symbol is set so that its area is proportional to the number of galaxies in the grid. The curve connects points where our morphology matches with RC3 morphology. A tight correlation is seen between the two classifications. For a given T(ours), the average discrepancy in the two classifications (in units of T_{RC3}) is $\langle |\Delta T_{RC3}| \rangle = 1.6$ with the rms scatter of 1.8. Naim et al. (1995) compared experts' classifications and concluded that the rms scatter among classifiers is 1.8.

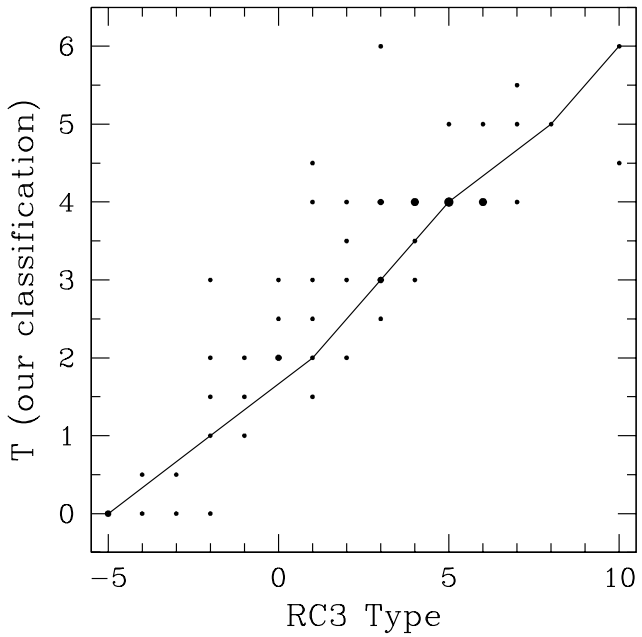

FIG. 3.—Morphology determined by our eye classification plotted against that given in RC3 for 54 common galaxies. The solid line connects points where our morphology matches with RC3 morphology.

A somewhat larger discrepancy between our classification and that given in RC3 may be expected, owing to the fact that we have estimated morphology from CCD images for which the contrast and gray scale are not fixed, whereas RC3 classification is based on photographic materials. On the other hand, Naim et al. used the identical prints for test classifications. In view of these considerations, we take our classification to be acceptable. In specific details, our classification tends to classify some S0 galaxies as E and classify spiral galaxies into somewhat later types.

Figure 4 shows the morphological-type distribution of galaxies in our sample. The relative fractions of types given in the literature (Fukugita, Hogan, & Peebles 1998; Loveday 1996) obtained in the B or b_J band are also plotted for comparison (normalized to the total number of galaxies in our sample). Loveday does not classify spiral galaxies into subclasses; so his numbers are distributed evenly over classes 2, 3, and 4. In our sample, the number of galaxies with $T = 0$ (i.e., E) is significantly higher than that of $T = 1$ (S0) galaxies, in contrast to the other results, implying that our classifiers set the division criterion of E and S0 to be more to the S0 side than in other work.[17] Taking $T < 1.5$ as early-type (E and S0) galaxies, the frequency of the early-type galaxies in our sample $0.34 = 154/456$ is consistent with what has been known from the work in the blue bands. In the following analysis, we mostly take E and S0 as a single class.

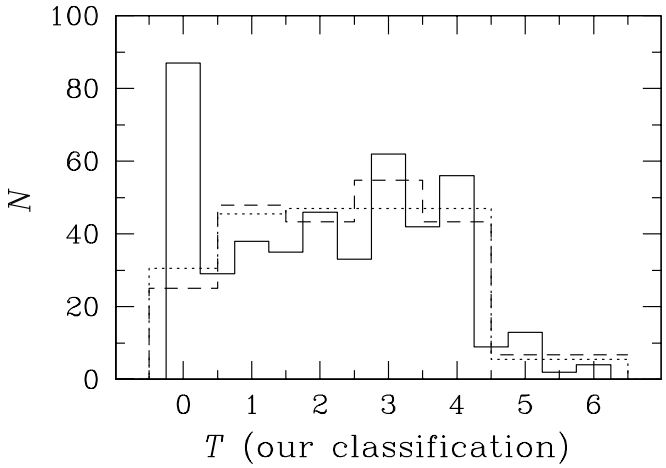

FIG. 4.—Distribution of morphological types for the 456 galaxies (*solid line*). The dotted line and dashed line indicate the type mixes given in Loveday (1996) and Fukugita et al. (1998), respectively.

To conclude this section, we quote the frequency of morphological types:

$$\mathrm{E} + \mathrm{S0}:\mathrm{Sa}:\mathrm{Sb}:\mathrm{Sc}:\mathrm{Sdm} + \mathrm{Im} = 0.34:0.18:0.21:0.21:0.06\ . \quad (4)$$

We do not detect any significant systematic change of morphological compositions with magnitude bins. So we regard this fraction to represent a fair value for field galaxies brighter than $r^* = 18$ mag.

4. COLOR INDICES

4.1. *Color Indices as a Function of Morphology*

In Figure 5, we plot (1) u^*-g^*, (2) g^*-r^*, (3) r^*-i^*, and (4) i^*-z^* colors against T. The size of the symbol is again set so that its area is proportional to the number of galaxies falling in the grid. The mean and rms of the color distributions are calculated in Table 1 and represented in Figure 6*a*–6*d*.[18] As noted in § 2, colors of each galaxy are measured for a common aperture, which is defined as $2 \times r_p(r^*)$. The aperture is reasonably large, so that our color indices are regarded as representing nearly those for the total flux. We correct all colors for Galactic reddening. The open squares connected by lines in Figures 5 and 6 are colors calculated convolving Kennicutt's (1992) spectrophotometric atlas of nearby galaxies with the responses of the SDSS photometric system to give broadband colors (Fukugita, Shimasaku, & Ichikawa 1995; hereafter FSI).

We indicate in Figure 6*a* representative uncertainties in our T measurements for early and late types by horizontal bars (the estimate at $T = 0$ and 3), which are estimated from the difference between our classification and that of RC3 shown in Figure 3.[19]

We observe (more clearly in Fig. 6) that the data are distributed fairly close to the FSI calculations for (1) u^*-g^*, (2) g^*-r^*, and (3) r^*-i^* colors. For g^*-r^*, the difference between the mean of the data and the calculation is less than 0.05, except for Im (a 0.3 mag discrepancy), for which the synthesis calculation uses the bluest known galaxies (NGC 4449 and NGC 4485) to define the envelope of the bluest color. The next largest discrepancy in g^*-r^* color is seen for elliptical galaxies: the data are redder than

[17] In a later work, we tried to reclassify the sample by resetting the division criterion in a way that the frequency of E:S0 agrees with more traditional values in the blue band, but we do not adopt this reclassification in the present paper.

[18] When calculating the mean, we dropped galaxies having too unrealistic colors; their colors are likely to be ascribed to errors due to unsuccessful deblending processes.

[19] The uncertainty we plotted here is the quadratic sum of the random and systematic errors around the RC3 type at a given T.

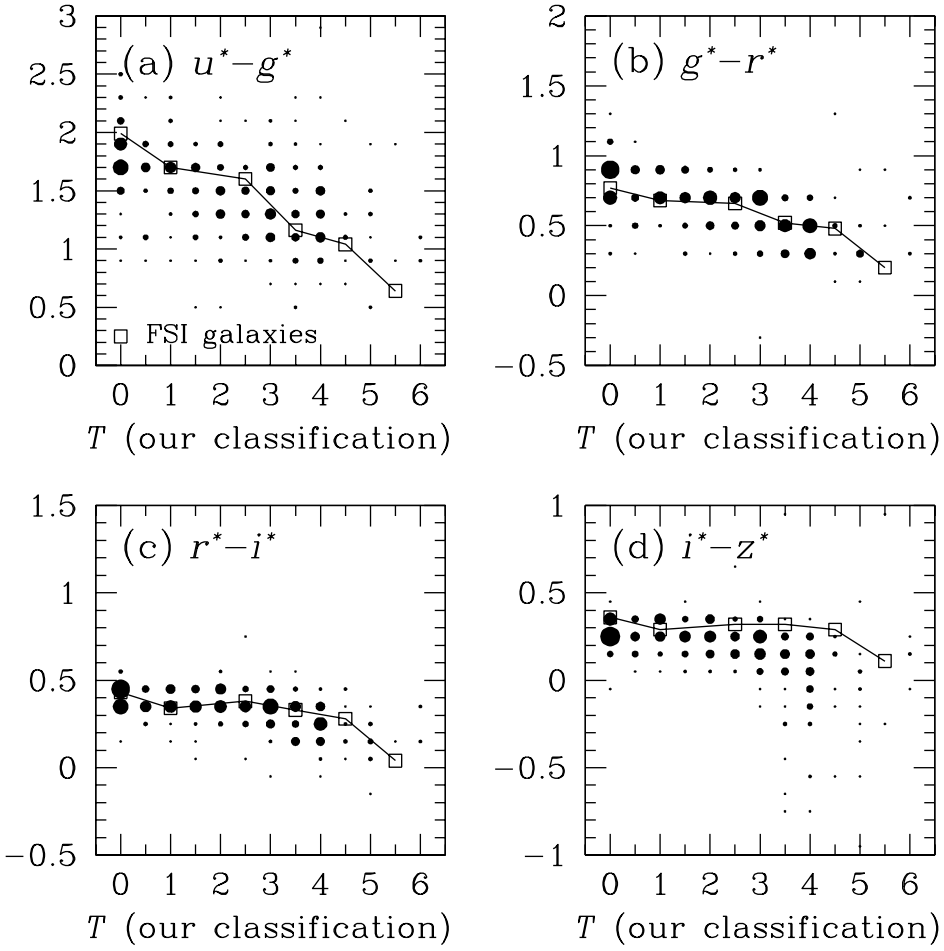

FIG. 5.—Colors of our galaxies plotted against morphology. Panels (*a*), (*b*), (*c*), and (*d*) are for $u'-g'$, $g'-r'$, $r'-i'$, and $i'-z'$, respectively. All colors have been corrected for Galactic reddening. The area of each filled circle is proportional to the number of galaxies falling into the grid. The open squares connected with solid lines indicate colors calculated (FSI) from Kennicutt's spectrophotometric atlas of nearby galaxies.

the synthesis calculation by 0.05 mag. This level of discrepancy, however, is seen for $B-V$ color of elliptical galaxies, either with Kennicutt's spectrophotometric data or with the spectroscopic energy distribution (SED) of Coleman, Wu, & Weedman (1980, hereafter CWW), when compared with the broadband color: the template SED of elliptical galaxies is not sufficiently red to give $B-V \simeq 1$ obtained by broadband photometry, as noted by FSI.

TABLE 1

MEAN COLORS OF SDSS GALAXIES AS A FUNCTION OF T

T	Hubble Type	u^*-g^*	g^*-r^*	r^*-i^*	i^*-z^*
$T < 0.5$	E	1.79 (0.26)	0.83 (0.14)	0.41 (0.05)	0.27 (0.06)
		86	87	87	87
$0.5 \le T < 1.5$.....	S0	1.66 (0.30)	0.75 (0.14)	0.38 (0.05)	0.26 (0.06)
		67	67	67	67
$1.5 \le T < 2.5$.....	Sa	1.49 (0.32)	0.68 (0.15)	0.38 (0.07)	0.25 (0.08)
		81	81	81	81
$2.5 \le T < 3.5$.....	Sb	1.40 (0.28)	0.62 (0.13)	0.35 (0.08)	0.20 (0.09)
		95	94	93	94
$3.5 \le T < 4.5$.....	Sc	1.28 (0.33)	0.46 (0.12)	0.27 (0.09)	0.07 (0.16)
		94	98	97	91
$4.5 \le T < 5.5$.....	Sdm	1.16 (0.38)	0.42 (0.24)	0.20 (0.12)	0.04 (0.20)
		22	22	21	18
$5.5 \le T$	Im	1.14 (0.33)	0.61 (0.23)	0.23 (0.08)	0.05 (0.17)
		6	6	5	5

NOTES.—The numbers in the parentheses are dispersions. The numbers in the second rows for each morphology listing are the number of galaxies used to calculate the mean. Only galaxies satisfying the following criteria are used to calculate the mean: $0 \le u^*-g^* \le 2.5$, $0 \le g^*-r^* \le 1.5, 0 \le r^*-i^* \le 1$, $-0.5 \le i^*-z^* \le 0.5$.

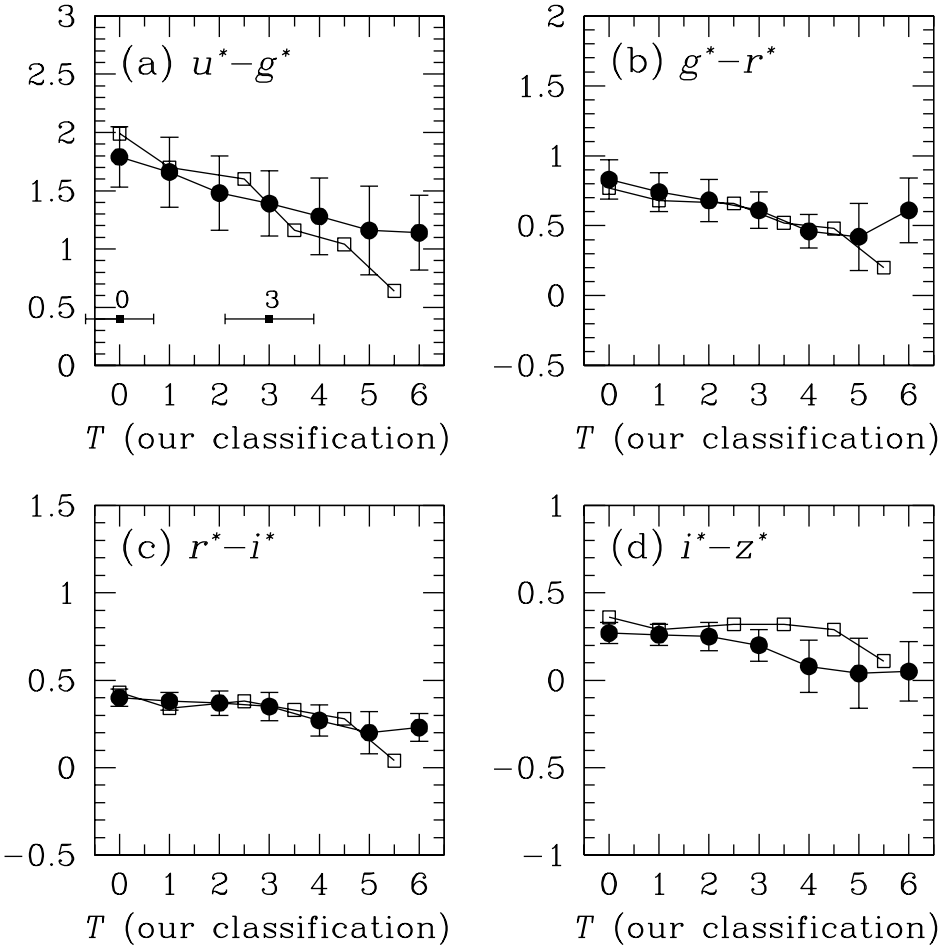

FIG. 6.—Mean and rms colors of dereddened galaxies plotted against morphology. Panels (*a*), (*b*), (*c*), and (*d*) are for $u'-g'$, $g'-r'$, $r'-i'$, and $i'-z'$, respectively. The open squares connected with solid lines indicate synthetic calculation of FSI. The two filled squares with error bars in (*a*) show the errors in T(ours) measurements at $T = 0$ and 3 estimated from the difference between our classification and that of RC3.

For r^*-i^* color, the difference between the data and the FSI synthetic colors is less than 0.04, again except for Im galaxies. The disagreement between our data and the FSI calculations is somewhat larger for u^*-g^*, but the scatter is wider for this color; we cannot conclude that the disagreement is significant. We remark, however, that the calculation being redder than observation by 0.2 mag for E galaxies may be ascribed to the use of metal-rich giant elliptical galaxies in constructing the composite SED. The u^*-g^* index is most sensitive to the metal abundance. For Im galaxies, the observed u^*-g^* color is redder than the calculation because of the use of a blue template object, as we have seen for the Im type in g^*-r^*.

A significant deviation is seen for the i^*-z^* color, for which the data are clearly bluer than the synthetic calculation by 0.1 mag for early-type galaxies and 0.2 for later type galaxies. While the SED that covers the z' band used in FSI relies on an extrapolation from the bluer wavelengths, we cannot blame this disagreement simply on an incorrect extrapolation, as we discuss in § 4.2.

We present in Figure 7 color-color diagrams (1) g^*-r^* versus u^*-g^*, (2) r^*-i^* versus g^*-r^*, and (3) i^*-z^* versus r^*-i^*. The dots represent each galaxy, and the curves are predictions from synthetic calculations of FSI (*filled squares*), CWW SEDs extended to the near infrared by Neugebauer (2000, private communication; *filled triangles*), both of which use empirical SED of galaxies, Kodama & Arimoto's (1997) stellar population synthesis model (*open squares*), and GISSEL of the Bruzual & Charlot (1996, in Leitherer et al. 1996; see also Bruzual & Charlot 1993) stellar population synthesis model (*open triangles*). The convergence of the four synthesis calculations is very good for the g^*-r^* versus u^*-g^* plot. A trend is visible that the SDSS photometry gives a somewhat bluer u^*-g^* (or slightly redder g^*-r^*) for early-type galaxies than all synthetic calculations. The agreement among synthetic calculations is still fairly good for the r^*-i^* versus g^*-r^* plot; the SDSS data also closely follow the synthetic calculations. In the i^*-z^* versus r^*-i^* plot, however, the data are clearly shifted by 0.1–0.2 mag downward (bluer i^*-z^*) compared with all four synthetic curves, which mutually agree very well.[20] The $i'-z'$ color of the SDSS galaxies is deviated from all model calculations.

4.2. *Comparison with Other Multicolor Broadband Photometry*

Buta & Williams (1995, hereafter BW) present VR_CI_C colors for 501 nearby galaxies classified into morphology according to the RC3 system. UBV colors for these galaxies

[20] This does not necessarily mean that model SEDs are correct, since they are not well constrained beyond i' passband.

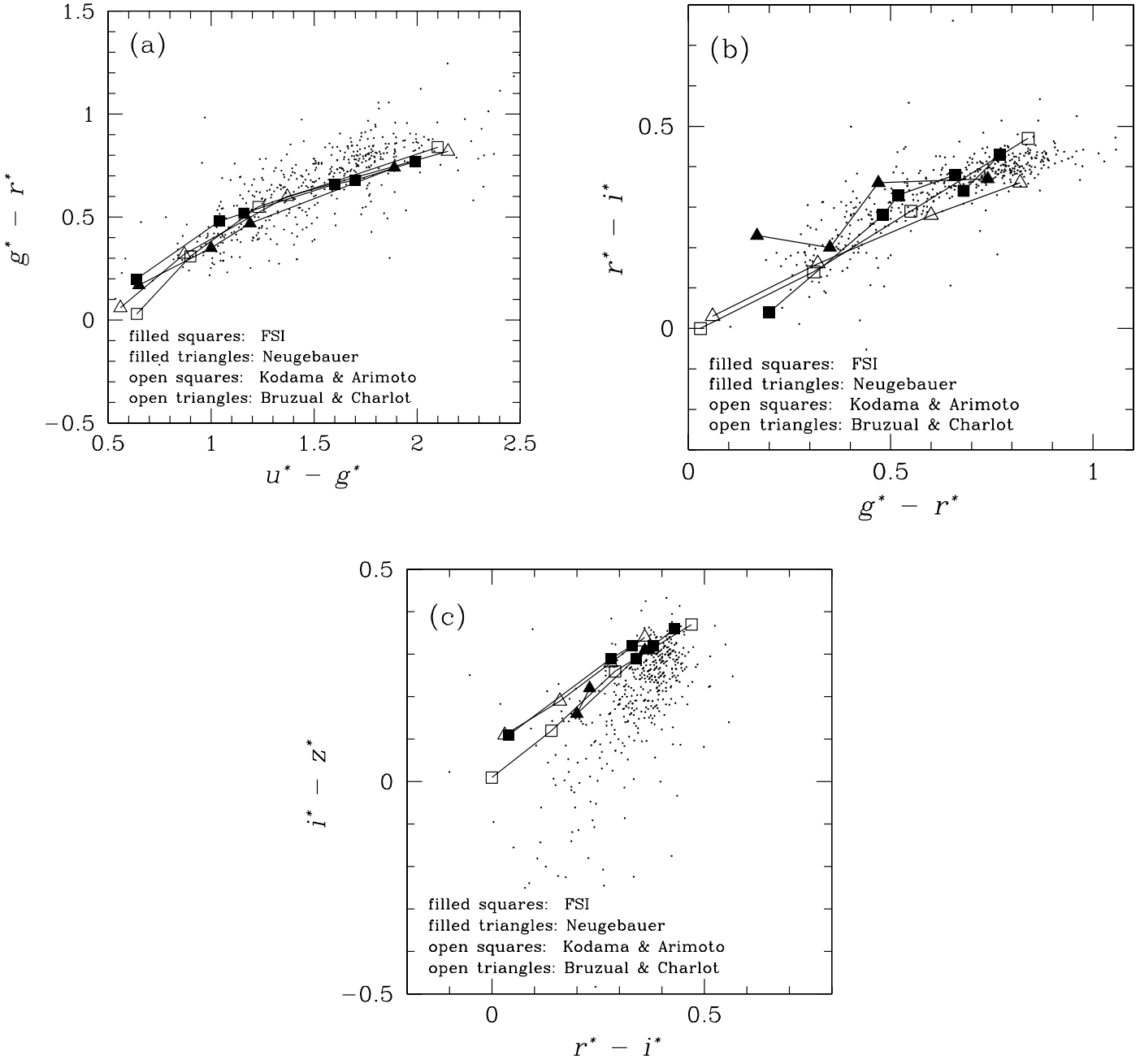

FIG. 7.—Color-color distributions of our galaxies: (*a*) $u'-g'$ vs. $g'-r'$; (*b*) $g'-r'$ vs. $r'-i'$; and (*c*) $r'-i'$ vs. $i'-z'$. The dots represent each galaxy, and the curves are predictions from synthetic calculations of FSI (*filled squares*), CWW SEDs extended to the near-infrared by Neugebauer (2000, private communication; *filled triangles*), Kodama & Arimoto's (1997) stellar population synthesis model (*open squares*), and GISSEL of Bruzual & Charlot's (1993) stellar population synthesis model (*open triangles*).

are given in RC3. In this subsection, we compare SDSS photometry with the BW (and RC3) catalog to examine the consistency among broadband photometries. Color transformations from the $UBVR_CI_C$ system to the SDSS system are carried out using the transformation laws given in FSI. The RC3 morphology indices are also converted into our system. We adopt BW's total color to compare with our Petrosian color. Figures 8*a*–8*d* give plots for the BW sample, similar to the plots in Figures 5*a*–5*d*. We remark that the BW sample is not homogeneous with respect to morphology but is highly biased toward early-type galaxies. We expect, however, that this does not produce any biases in our color analysis. We overlay the data of our sample (Fig. 5; we omit $T = 0.5$ and 1.5 data, since no galaxy is classified as these types in the BW sample) by open circles, with a horizontal offset of $+0.2$ for clarity.

A comparison of Figure 8 with Figure 5 shows that the $u'-g'$, $g'-r'$, and $r'-i'$ distributions of the BW galaxies are grossly consistent with those for SDSS photometry. The agreement of the $u'-g'$ colors between the two samples is particularly good, although a somewhat smaller scatter for the early-type galaxies of the BW sample may be ascribed to its selection effect that the BW sample is not homogeneous. The $g'-r'$ and $r'-i'$ colors for early-type galaxies are slightly bluer for the BW sample. The appreciable discrepancy found in the comparison of the two samples is with $i'-z'$ colors. In the SDSS sample, $i'-z'$ colors are systematically bluer than those of BW by $\sim$0.1–0.2 mag. This trend is

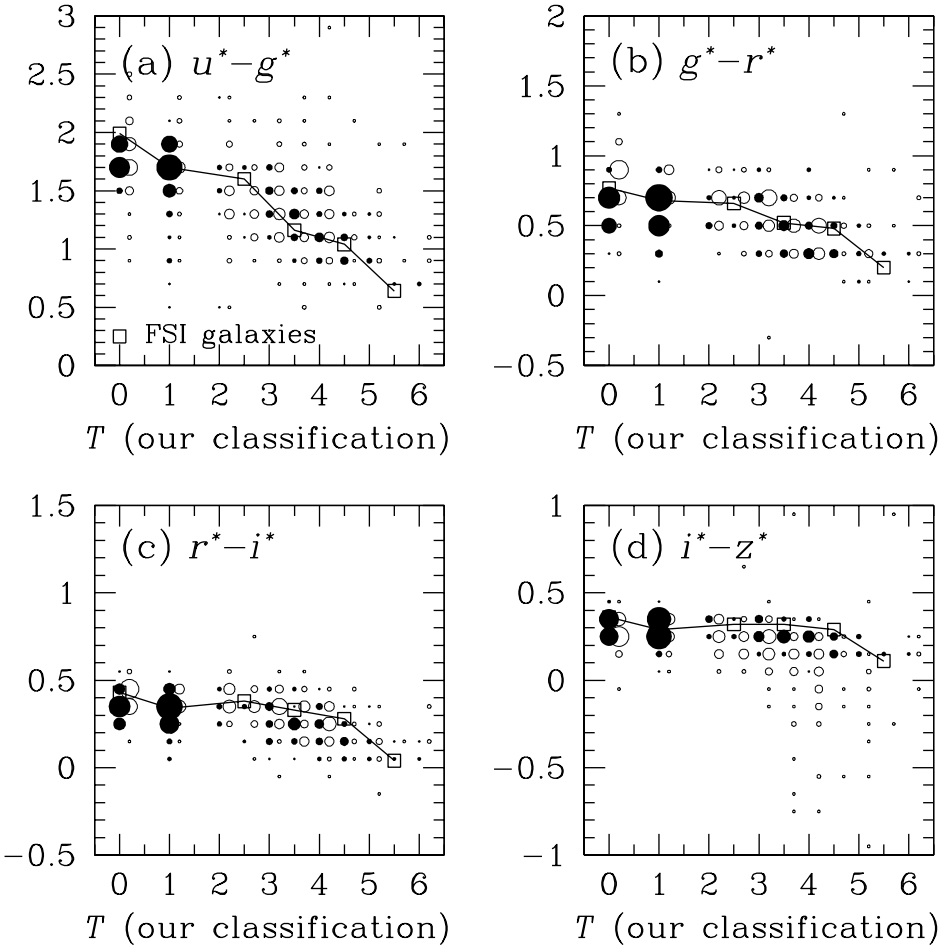

FIG. 8.—Same as Fig. 5, but for Buta & Williams's (1995) galaxies. Overlaid are the plots for our sample (Fig. 5), marked by open circles with a horizontal offset of +0.2 for clarity.

similar to what was found between the FSI calculation and the SDSS measures of galaxies in the previous subsection.

This discrepancy in $i'-z'$ color leads us to suspect that there may be a systematic error by 0.1–0.2 mag in z'-band photometry, but the real reason is not clear to us. The preliminary work for the SDSS primary standard stars (Smith et al. 2000) shows that all SDSS color indices relative to the Johnson-Morgan-Cousins photometric system differ from a synthetic calculation using Gunn-Stryker stars (Gunn & Stryker 1983) by no more than 0.03 mag. We have recently recognized some unexpected shifts of the filter response function in the 2.5 m camera system due to the evaporation of water vapor from silicon layer of the coating surface when the filters are soaked in a vacuum chamber, but we estimate the effect to be smaller than 0.015 mag for all color bands. The difference in the response between the front-illuminated thick CCD device used in the 2.5 m camera and the back-illuminated thin device for the Photometric Telescope (which defines the SDSS magnitude) does not cause an offset of more than 0.01 mag. The sky brightness and its time variation are the highest in the z' band, so errors in the sky subtraction in z' band could affect photometry of galaxies. However, it is not easy to estimate photometric errors due to the sky subtraction errors, since they affect galaxy photometry in a complicated way depending on sizes and surface brightnesses of galaxies. At present, we have not found clear evidence that they account for the discrepancy in $i'-z'$ color. It is worth noting, however, that the observed amount of the discrepancy in $i'-z'$ does not depend either on the brightness (and size) of galaxies nor on the position of galaxies on a strip (i.e., when they were imaged). The effect of 0.1–0.2 mag seems a bit too large to be ascribed to the uncertainties in the present photometric system, but we cannot find the reason for this discrepancy at the moment.

5. SCALE LENGTHS

In this section, we study the relation between apparent size and apparent brightness of galaxies. We expect different relations for different morphological types. The relation may also depend on the color band used if star-forming regions or metallicity distributions are not homogeneous throughout the galaxy. The information on the radius-brightness relation is also needed to construct a realistic simulation of galaxies. In addition, we examine whether the relation derived from SDSS photometry is consistent with our knowledge of the galaxy sizes we obtained from other studies of local galaxies. The consistency would allow us to supplement the SDSS data with the results from other more detailed studies, including galaxies that have not yet been studied by SDSS.

We consider r_{50} estimated in the five color bands as a measure for the galaxy size. Note that r_{50} is approximately the conventionally defined effective radius (half-light radius).

We adopt Petrosian magnitudes m_P in the five color bands as well to represent apparent brightness.

The four panels in Figure 9 show the plot of $r_{50}(\lambda_i)$ ($\lambda_i = u', g', r'$, and i') as a function of apparent brightness in the r' passbands. We divide our galaxy sample into three morphological classes on the basis of T values: the open circles are early-type galaxies with $T < 1.5$ (E and S0 galaxies), the filled circles denote $1.5 \leq T < 4$ (S0/a to Sbc), and the crosses are for late spiral galaxies with $T \geq 4$ (later than Sc). The data are well represented by the curve

$$\log r_{50}(\lambda_i)'' = -0.2[m_P(\lambda_j) - 16 \text{ mag}] + a_{ij}\,, \qquad (5)$$

where a_{ij} are constants that depend on λ_i and λ_j. This relation holds for any combination of the passbands λ_i, λ_j, with the parameters a_{ij} (and their rms scatters) being obtained by least-squares fits to the plots for the three morphological classes. These parameters are given in Table 2 for $\lambda_i = u', g', r', i', z', \lambda_j = r'$, and for $\lambda_i = \lambda_j = u', g', r', i', z'$.

The plots in Figure 9 show that half-light Petrosian radii r_{50} are nearly independent of the color bands with which these radii are calculated. Looking into details, however, we see the trend that the half-light radius shrinks slightly from UV to redder bands for all morphological types (see rows 1–5 of Table 2). For early-type galaxies, we observe a 10% decrease in the effective radius continuously from the u' to the z' band. This is interpreted as due to the effect of the color gradient of early-type galaxies driven from the metallicity gradient. For spiral galaxies, the decrease is 20%–25%. This represents the star-forming component being more extended toward outer parts of galaxies: in other words, the increasing dominance of the bulge component in redder passbands.

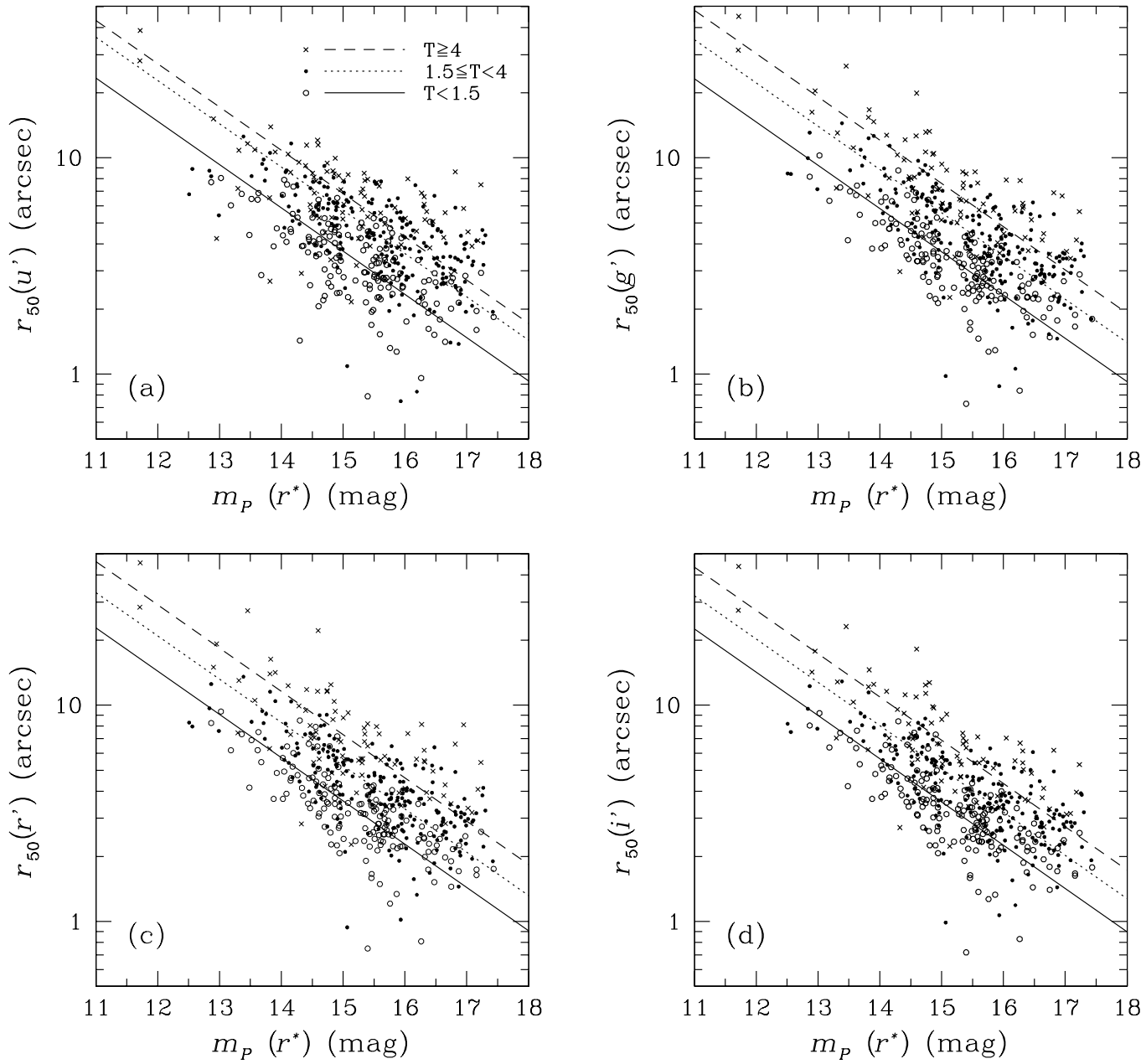

FIG. 9.—Half-light Petrosian radii measured in u' (*a*), g' (*b*), r' (*c*), and i' (*d*), plotted as a function of Petrosian magnitude in the r' band. Magnitudes have been corrected for Galactic extinction. Open circles, filled circles, and crosses indicate $T < 1.5$, $1.5 \leq T < 4$, and $T \geq 4$, respectively. The solid, dotted, and dashed lines in each panel show the best fit of eq. (5) to the three morphological classes of galaxies, respectively.

TABLE 2

FIT COEFFICIENTS a_{ij} IN THE RELATION BETWEEN APPARENT HALF-LIGHT RADIUS AND APPARENT BRIGHTNESS

No.	λ_i	λ_j	All	$T < 1.5$	$1.5 \le T < 4$	$T \ge 4$
1	u'	r'	0.51 (0.19)	0.37 (0.15)	0.56 (0.16)	0.63 (0.20)
2	g'	r'	0.51 (0.18)	0.36 (0.12)	0.55 (0.14)	0.68 (0.17)
3	r'	r'	0.49 (0.18)	0.36 (0.12)	0.52 (0.14)	0.66 (0.17)
4	i'	r'	0.48 (0.17)	0.35 (0.12)	0.51 (0.14)	0.64 (0.16)
5	z'	r'	0.44 (0.16)	0.33 (0.12)	0.47 (0.14)	0.57 (0.16)
6	u'	u'	0.94 (0.16)	0.87 (0.15)	0.96 (0.14)	0.99 (0.17)
7	g'	g'	0.64 (0.16)	0.52 (0.13)	0.67 (0.13)	0.77 (0.16)
8	r'	r'	0.49 (0.18)	0.36 (0.12)	0.52 (0.14)	0.66 (0.17)
9	i'	i'	0.41 (0.18)	0.27 (0.12)	0.44 (0.14)	0.59 (0.17)
10...	z'	z'	0.34 (0.19)	0.20 (0.12)	0.36 (0.16)	0.53 (0.19)

NOTES.—See eq. (5) for the definition. The numbers in parentheses are dispersion around the fit.

The fitting formulae with $i = j$ give useful parameters (see rows 6–10 of Table 2) to construct simulations of galaxies. The knowledge of these parameters is particularly important in understanding the detection limit of galaxies and the performance of star-galaxy classification.

Let us now investigate the consistency of equation (5) with the relation involving the effective radius known in the literature. The most accurate study concerning the scale of galaxies is presented by Kent (1985) on the basis of excellent Thuan-Gunn r-band CCD images of nearby bright galaxies with known redshifts. He derived the relations between intrinsic size and surface brightness separately for the bulge and disk components. Using the transformation law of FSI, we convert his relations between the effective radius (kiloparsecs) and the effective surface brightness (magnitudes per square arcsecond) to those in the SDSS r' band as

$$\mu_e = 2.5 \log [r_e \text{ (kpc)}] + 20.3(\text{mag s}^{-2}), \text{ (E, S0)}, \quad (6)$$

$$\mu_e = 2.5 \log [r_e \text{ (kpc)}] + 20.5(\text{mag s}^{-2}), \text{ (disks)}, \quad (7)$$

where we have assumed the Hubble constant to be 100 km s^{-1} Mpc^{-1}.

When these relations are fitted to the SDSS data for $T < 1.5$ (bulge dominated) and $T \ge 4$ (disk dominated), we obtain for the effective radius r_e defined by $I(r) \propto \exp [-0.7289(r/r_e)^{1/4}]$ for the de Vaucouleurs profile and the scale length defined by $I(r) \propto \exp(-r/h)$ for the exponential disk,

$$r_e = 2.56^{+0.81}_{-0.62} \text{ kpc (de Vaucouleurs profile)} \quad (8)$$

and

$$h = 2.62^{+0.83}_{-0.63} \text{ kpc (exponential disk)}, \quad (9)$$

where the errors indicate the 1 σ range. Note that the average luminosity of galaxies that contribute to galaxy number counts in the bright magnitude is very close to L^* (within ± 0.1 mag error for $r^* = 15$–18 mag) with the slope of the Schechter function $\alpha = -1.2$. Therefore, the values given in equations (8) and (9) represent the average sizes for the L^* galaxies.

Our data indicate that the mean h derived from late-type disks is about the same value as the mean r_e of early-type galaxies. With these two parameters, our data are consistent with the relations derived by Kent (1985).

6. CONCENTRATION INDEX

We define the (inverse) concentration index by the ratio of the two Petrosian radii $C = r_{50}/r_{90}$ measured in the r' band. Figure 10 shows C against T (see also Table 3). We have dropped 30 galaxies having $r_{50} < 2''$, since large smearing effects are suspected for C for such small galaxies unless significant corrections are made for the seeing (average FWHM is $\sim 1''.5$). The two filled squares with error bars near the top of the panel show the typical errors in T(ours) measurements at $T = 0$ and 3.

A tight correlation is seen between C and T; C increases with T, which is understood by the spheroid or bulge dominance of early-type galaxies and an increasing disk dominance of later type galaxies. We have studied similar plots for galaxies with magnitudes divided into three bins, $r^* < 16$, $16 < r^* < 17$, and $17 < r^* < 18$. No systematic

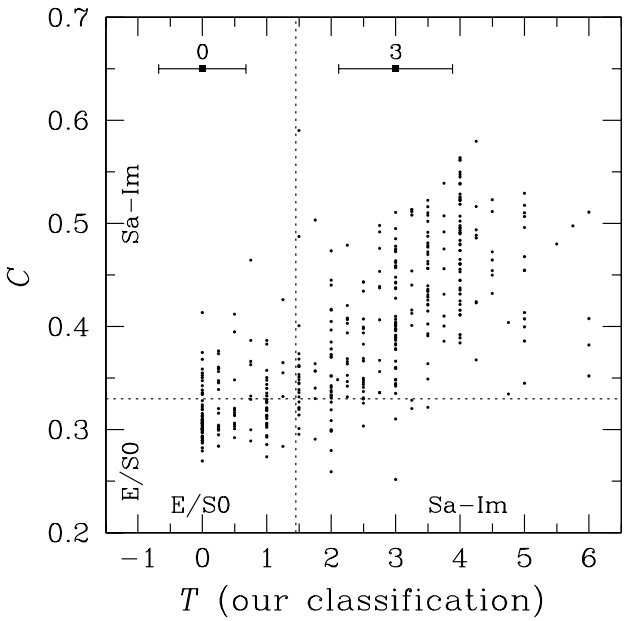

FIG. 10.—Concentration index C plotted against eye morphology T for 426 galaxies having $r_{50} \ge 2''$. The vertical line indicates the boundary which divides E/S0 galaxies and spiral/Im galaxies on the basis of eye morphology. The horizontal line is for the boundary accepted in the text ($C_1 = 0.33$) dividing low-C ("early-type") and high-C ("late-type") galaxies. The two filled squares with error bars near the top of the panel show the errors in T(ours) measurements at $T = 0$ and 3 estimated from the difference between our classification and that of RC3.

TABLE 3

CONCENTRATION INDEX $C = r_{50}/r_{90}$

		C	
T(our)	N	Mean	rms
$T < 0.5$	80	0.317	0.027
$0.5 \le T < 1.5$	56	0.331	0.037
$1.5 \le T < 2.5$	73	0.362	0.054
$2.5 \le T < 3.5$	92	0.404	0.057
$3.5 \le T < 4.5$	97	0.467	0.052
$4.5 \le T < 5.5$	22	0.452	0.055
$5.5 \le T$	6	0.439	0.061

effects are observed among the samples with different apparent brightnesses (hence different apparent sizes) of galaxies, in so far as we limit ourselves to galaxies with $r_{50} \geq 2''$. The galaxies with $r_{50} < 2''$ show a weaker correlation between C and T due to smearing by seeing but also possibly due to errors of eye classification.[21]

The scatter in C for a given T is larger than expected from the errors in our T measurements. This reflects the fact that galaxies with a given morphology have a fairly wide range in the bulge-to-disk ratio (e.g., Kent 1985; Simien & de Vaucouleurs 1986; Kodaira, Watanabe, & Okamura 1986), and the bulge-to-disk ratio is directly related to the concentration index.

We examined the correlations of visual morphology with a number of parameters measured by PHOTO (likelihoods of a fitting to the de Vaucouleurs or exponential profiles, texture parameters defined by PHOTO) in addition to the three parameters studied in this paper. The correlation of the likelihood of profile fitting and of the texture parameter with our visual morphology is not strong (we used the version of PHOTO version 5.0.3 of late 1999). The concentration index shows the strongest correlation with visual morphology, and a combination of the concentration index with other parameters, such as surface brightness, color, asymmetry parameter, does not appreciably enhance the correlation.

The concentration index is perhaps the best parameter to be used to classify morphology of galaxies. This is basically the same conclusion as reached by Doi et al. (1993) and further corroborated by Abraham et al. (1994). These authors used a combination of a concentration index and mean surface brightness, while the concentration index is sufficient for our case. This simplification arises merely from the different definition of the concentration indices. In Doi et al. and Abraham et al., the concentration index is defined using isophotal photometry. The calculated index then depends on both apparent brightness and distance of galaxies. To correct for these redundant effects, the second parameter is needed, and those authors took average surface brightness, which also depends on apparent brightness and the distance. In our case, the Petrosian quantities are physically well defined, independent of the apparent brightness or the distance. Therefore, the introduction of a second parameter is unnecessary.

The correlation in Figure 10 suggests that the C parameter can be used for morphological classification, allowing for the uncertainty of roughly $\Delta T \sim 1.5$ (see Table 3). The most important problem in the classification using the C parameter is that the C parameter for Sa galaxies can be as small as that for E galaxies, making it difficult to construct a purely early-type galaxy sample free of a contamination of Sa galaxies. As noted above, this problem is not ameliorated with the use of any second parameters we studied. On the other hand, the distinction between S0 and Sa is not too difficult, allowing for some intermediate cases, upon visual inspections because of the presence of spiral arms and/or H II regions in Sa galaxies, which are not properly picked up with the parameters given by PHOTO.

[21] We have examined whether highly inclined galaxies would disturb the correlations between C and T. We have found that the correlation does not change appreciably against the sample with specified minor-to-major axis ratio. Our concentration index defined using the Petrosian radii is a robust indicator against inclination of galaxies.

A practically important application is to distinguish E/S0 galaxies from spiral galaxies. Here we consider this problem in a more quantitative way and study the completeness and contamination of the morphologically classified sample with the use of the C parameter. The top panel of Figure 11 shows the completeness as a function of C: the solid curve represents the completeness of early-type galaxies when sample is selected with $C < C_1$ for a given C_1, while the dashed curve represents the completeness of the late-type galaxy sample with $C \geq C_1$. The completeness of the two samples balances with $C_1 = 0.35$ at 80%. On the other hand, the bottom panel of Figure 11 indicates the contamination from the opposite type. Namely, the solid curve is the contamination from late-type galaxies to the early-type galaxy sample with $C < C_1$. The dashed curve is the contamination by early-type galaxies to the late-type sample with $C \geq C_1$. The two curves become even at $C_1 = 0.32$.

The inspection of two curves in the bottom panel of Figure 11 shows that we can make a reasonably pure late-type galaxy sample with the choice of large C_1, say, 0.37 at a loss of completeness (70% completeness; contamination is less than 5%). The opposite is not true: one cannot decrease the contamination of an early-type sample by late-type galaxies below 15%, whatever value of C_1 is chosen, as a result of a contamination from Sa galaxies.[22]

Our recommended choice of C_1 is 0.33, if we want dichotomous classification of galaxies into early and late types. For this specific choice, the completeness and contamination are given in Table 4. Out of the 136 early-type (E/S0) galaxies, 93 are classified as "early" types, i.e., a completeness of 68%. On the other hand, 24 "early"-type galaxies are not real E/S0 galaxies, which means a contamination of 21% (24/117). Similarly, the fraction of late-type

[22] We suspect that this contamination is not due to Seyfert galaxies, since the color of the contaminants are not bluer than others.

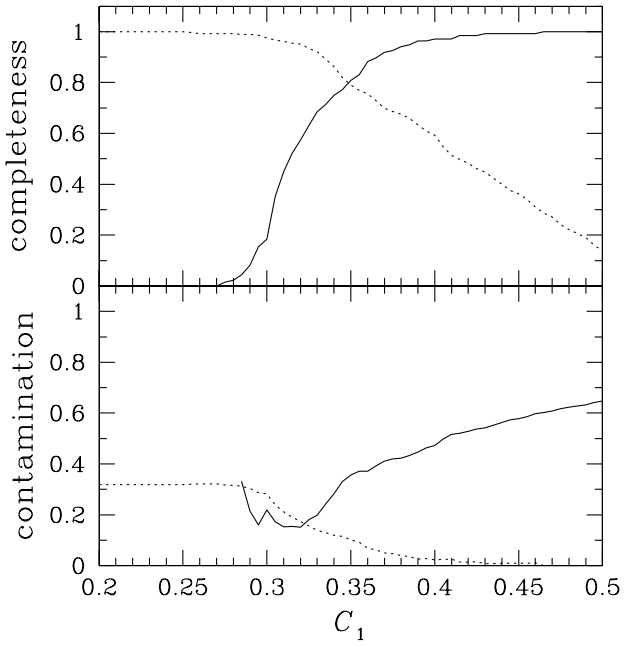

FIG. 11.—Completeness and contamination of early- and late-type galaxies as a function of C_1. The solid and dotted lines are for early- and late-type galaxies, respectively.

TABLE 4

CORRELATION BETWEEN EYE MORPHOLOGY AND THAT CLASSIFIED WITH THE CONCENTRATION INDEX WITH $C_1 = 0.33$

Parameter	$T < 1.5$	$T \geq 1.5$	Sum	Contamination (%)
"Early-type" galaxies.....	93	24	117	21
"Late-type" galaxies.....	43	266	309	14
Sum.....	136	290	426	
Completeness (%)	68	92	...	...

(Sa-Im) galaxies classified as "late" types is 92% (266/290) and the contamination in the "late" galaxy sample from early-type galaxies is 14% (43/309).

In summary, our analysis demonstrates that the parameter $C = r_{50}/r_{90}$ is useful for automated classification of early- and late-type galaxies, if one is satisfied with a completeness of $\simeq$70%–90%, allowing for a contamination of $\simeq$15%–20%. It appears difficult to improve the performance with the use of simple photometric parameters. Further improvement requires the introduction of more complicated parameters such as those characterizing the presence of spiral arms and H II regions. An improvement of late-type galaxy classification may be achieved with the introduction of the asymmetry parameter (e.g., Abraham et al. 1996).

7. CONCLUSIONS

We have produced a morphologically classified sample of 456 bright galaxies from imaging data that were taken during the Sloan Digital Sky Survey commissioning phase. We have classified galaxies into seven Hubble types (E, S0, Sa, Sb, Sc, Sdm, and Im) by visual inspections carried out by four individuals. We have measured the distributions of colors, scale lengths, and concentration indices in the SDSS photometric system as functions of morphology. Our prime purposes are (1) to derive the fundamental statistical properties of galaxies in the SDSS passbands, (2) to examine the consistency with existing galaxy data other than the SDSS, and (3) to find the parameters that can be used for an efficient automated morphological classifier. All parameters we have studied in this paper, except for visually determined morphology, are among the standard outputs from the SDSS image analysis software (PHOTO) and thus routinely registered in the SDSS photometric catalog.

We have found that the colors of our galaxies in the SDSS system match with those obtained from template SED data and from $UBVR_CI_C$ broadband photometry of nearby galaxies to within $\approx$0.05 mag. The exception is $i' - z'$ color for which the discrepancy is as large as 0.1–0.2 mag. We could not find the origin of this discrepancy yet.

We found that the half-light radius falls on the line $\log r_{50} = -0.2m + \text{const}$, and the constant we found indicates $r_e \simeq 2.6$ kpc for de Vaucouleurs profiles and $h \simeq 2.6$ kpc for exponential disks of late-type spiral galaxies, with the aid of the surface brightness radius relation derived by Kent (1985). We also found that the half-light radius of galaxies depends slightly on the color band, and the dependence is consistent with the expected distribution of star-forming regions for late-type galaxies and with the known color gradient in early-type galaxies.

Finally, we have shown that the concentration index shows a strong correlation with the morphological types. We explored the possibility of using this parameter for automated morphological classification of galaxies in order to classify a huge number of galaxies into early, intermediate, and late types with parameters that are routinely produced in the photometric data processing of the SDSS. For an optimum ratio of $(r_{50}/r_{90})_1 \equiv C_1 = 0.33$, we find, however, a 15%–20% contamination from opposite types of galaxies. The contamination is particularly important for the early-type galaxy sample, and we must consider some higher order photometric parameters to enhance the performance.[23]

We thank the referee, Roberto Abraham, for useful comments. The Sloan Digital Sky Survey (SDSS) is a joint project of the University of Chicago, Fermilab, the Institute for Advanced Study, the Japan Participation Group, the Johns Hopkins University, the Max-Planck-Institute for Astronomy, the Max-Planck-Institute for Astrophysics, New Mexico State University, Princeton University, the US Naval Observatory, and the University of Washington. Apache Point Observatory, site of the SDSS telescopes, is operated by the Astrophysical Research Consortium (ARC). Funding for the project has been provided by the Alfred P. Sloan Foundation, the SDSS member institutions, the National Aeronautics and Space Administration, the National Science Foundation, the US Department of Energy, the Japanese Monbukagakusho, and the Max Planck Society.

[23] PHOTO has been continuously updated over the years. After we submitted our paper, Strateva et al. (2001) found on the basis of a different sample (287 galaxies at $g^* < 16$) that the likelihood of profile fitting based on a later version of PHOTO (5.2) correlates with eye morphology better than we found. However, they also found that the profile fitting does not work well in comparison with concentration index for bright galaxies such as those we study in our paper.

REFERENCES

Abraham, R. G., Tanvir, N. R., Santiago, B. X., Ellis, R. S., Glazebrook, K., & van den Bergh, S. 1996, MNRAS, 279, L47
Abraham, R. G., Valdes, F., Yee, H. K. C., & van den Bergh, S. 1994, ApJ, 432, 75
Bruzual, A. G., & Charlot, S. 1993, ApJ, 405, 538
Buta, R., & Williams, K. L. 1995, AJ, 109, 543 (BW)
Coleman, G. D., Wu, C.-C., & Weedman, D. W. 1980, ApJS, 43, 393 (CWW)
de Vaucouleurs, G. 1948, Ann. d'Astrophys., 11, 247
de Vaucouleurs, G., de Vaucouleurs, A., Corwin, H., Jr., Buta, R., Paturel, G., & Fouqué, P. 1991, Third Reference Catalogue of Bright Galaxies (New York: Springer) (RC3)
Doi, M., Fukugita, M., & Okamura, S. 1993, MNRAS, 264, 832
Frei, Z., & Gunn, J. E. 1994, AJ, 108, 1476
Fukugita, M., Hogan, C. J., & Peebles, P. J. E. 1998, ApJ, 503, 518
Fukugita, M., Ichikawa, T., Gunn, J. E., Doi, M., Shimasaku, K., & Schneider, D. P. 1996, AJ, 111, 1748
Fukugita, M., Shimasaku, K., & Ichikawa, T. 1995, PASP, 107, 945 (FSI)
Fukugita, M., et al. 2001, in preparation
Gunn, J. E., et al. 1998, AJ, 116, 3040
Gunn, J. E., & Stryker, L. L. 1983, ApJS, 52, 121
Kennicutt, R. C. 1992, ApJS, 79, 255
Kent, S. M. 1985, ApJS, 59, 115
Kodaira, K., Watanabe, M., & Okamura, S. 1986, ApJS, 62, 703
Kodama, T., & Arimoto, N. 1997, A&A, 320, 41
Lahav, O., Naim, A., Sodré, L., Jr., & Storrie-Lombardi, M. C. 1996, MNRAS, 283, 207
Leitherer, C., et al. 1996, PASP, 108, 996
Loveday, J. 1996, MNRAS, 278, 1025
Lupton, R. H., et al. 2001, in preparation

Morgan, W. W. 1958, PASP, 70, 364
Naim, A., et al. 1995, MNRAS, 274, 1107
Sandage, A. 1961, The Hubble Atlas of Galaxies (Washington: Carnegie Inst. Washington)
Schlegel, D. J., Finkbeiner, D. P., & Davis, M. 1998, ApJ, 500, 525
Simien, F., & de Vaucouleurs, G. 1986, ApJ, 302, 564
Smith, J. A., et al. 2000, AAS Meeting, 197, 1311
Strateva, I. V., et al. 2001, AJ, in press
Yasuda, N., et al. 2000, AJ, in press
York, D. G., et al. 2000, AJ, 120, 1579